Journal of Alloys and Compounds 524 (2012) 1–4

Contents lists available at SciVerse ScienceDirect

Journal of Alloys and Compounds

journal homepage: www.elsevier.com/locate/jallcom

Multi-resonances behavior of Ni nanobelt/paraffin composites at microwave frequencies

T. Liu, P.H. Zhou*, D.F. Liang, J.L. Xie, L.J. Deng

State Key Laboratory of Electronic Thin Films and Integrated Devices, University of Electronic Science and Technology of China, Chengdu 610054, People's Republic of China

ARTICLE INFO

Article history:
Received 25 October 2011
Received in revised form 5 January 2012
Accepted 31 January 2012
Available online 14 February 2012

Keywords:
Ni nanobelt
Natural resonance
Non-uniform exchange resonance
Maxwell–Garnett mixing rule
Landau–Lifshitz–Gilbert equation

ABSTRACT

Ni nanobelts are synthesized through a facile hydrothermal method to form magnetic composites for high frequency applications. Four resonance peaks of the relative complex permeability illustrate the multi-resonance behavior in Ni nanobelt/paraffin composites in a frequency range of 2–18 GHz. The resonance absorption characteristics are analyzed by fitting the permeability spectrum with the well-known Landau–Lifshitz–Gilbert (LLG) equation and Maxwell–Garnett mixing rule. Unlike previous studies, LLG equation has been deduced on account of the random distribution of Ni nanobelts in paraffin matrix first, and then applied for data fitting and resonance identification. Correspondingly, the first band is attributed to natural resonance, while the other three bands are considered to originate from non-uniform exchange resonance.

1. Introduction

Both theoretical analysis and experimental studies indicate that control of the morphology of ferromagnetic particles is important since resonance frequency of the composites consisting of these particles is highly dependent on the particle shape due to demagnetization anisotropy [1–4]. The anisotropic particles may have a higher resonance frequency and exceed Snoek's limit in the gigahertz frequency range [5]. Nickel is one of the most important ferromagnetic materials. As a new type of nanostructure, Ni nanobelts have been prepared by the high-yield hydrothermal reduction method recently and their static magnetic characteristics have been analyzed accordingly. However, scientific attention has been rarely devoted to the investigation of the dynamic magnetic properties of Ni nanobelts or its composites to date. In the present paper, the relative complex permeability of Ni nanobelt/paraffin composites is measured in the wide frequency range of 2–18 GHz, and the multi-resonance behavior of composites has been detected. The permeability spectra are fitted with the LLG equation and Maxwell–Garnett mixing rule to investigate the working mechanism. Modifications on LLG equation have been made by taking into account of the random distribution of the Ni nanobelts in the paraffin matrix. Both the measured results and the theoretical predictions are discussed.

2. Experiment and characterization

Ni nanobelts were prepared by the facile hydrothermal method, and the detailed synthesis procedure has been described in Ref. [6]. SEM images of the sample were shown in Fig. 1a and b. The products mainly consist of belt-like particles with lengths up to several tens micrometers, width ranging from several hundreds to one thousand nanometers and thickness as thin as ~10 nm. XRD pattern in Fig. 1c confirms the face-centered cubic (fcc) phase of Ni nanobelts with an average grain size estimated to be 13.8 nm by the Scherrer formula. Magnetic hysteresis loops of the samples were presented in Fig. 1d. It is shown that the saturation magnetization (M_S) and coercivity (H_c) for the Ni nanobelts were 40.5 emu/g and 259.67 Oe, respectively. The atoms of the surface layer in less ordered spin arrangement [7] and the ultrathin surface oxidation cause the decrease of the saturation magnetization of the Ni nanobelt compared with bulk Ni. The measured H_c is apparently larger than that of the bulk one (200 Oe) [8]. This may be attributed to the introduction of shape anisotropy in the nanobelt structure. The Ni nanobelt/paraffin composite sample was prepared by randomly and uniformly dispersing the Ni nanobelt powders (16.83 vol%) in paraffin and was then pressed into toroidal shape with an inner diameter of 3.04 mm and outer diameter of 7 mm. Electromagnetic parameters of the toroidal shape sample were measured

* Corresponding author..
E-mail address: zhouph1981@163.com (P.H. Zhou).

0925-8388/$ – see front matter © 2012 Elsevier B.V. All rights reserved.
doi:10.1016/j.jallcom.2012.01.157

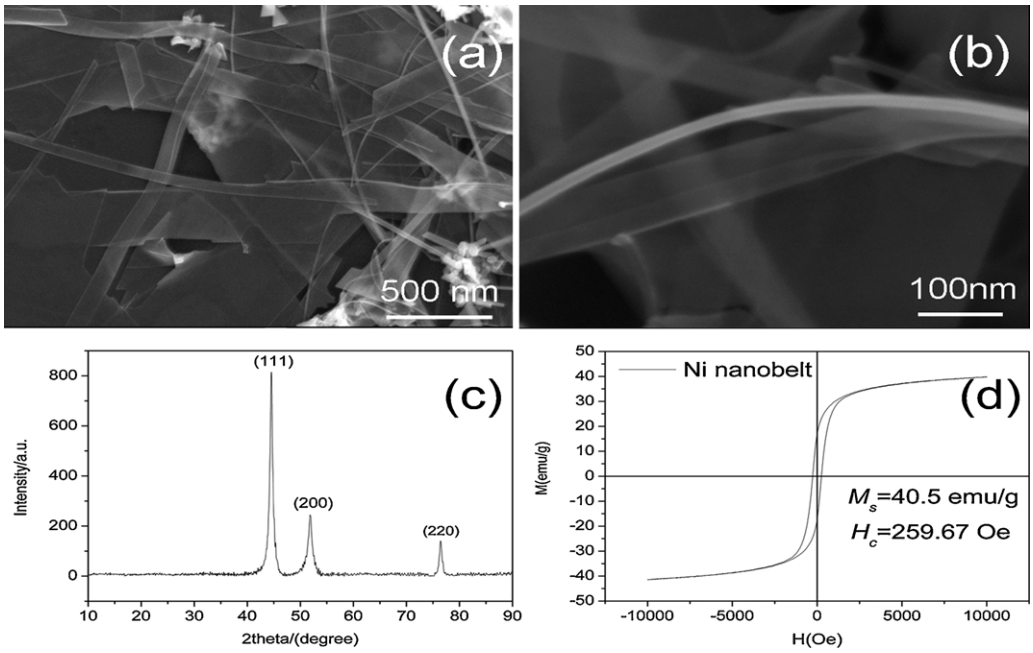

Fig. 1. Characteristic pictures of Ni nanobelts at low magnification (a) and high magnification (b). XRD pattern of Ni nanobelt (c). Magnetic hysteresis loops measured at room temperature (d).

in the 2–18 GHz range using an Agilent 8720ET network analyzer.

3. Theoretical prediction

3.1. The mechanism of multi-resonance

Fig. 2 illustrates the experimental curves of the effective permeability of the composites with 16.83 vol% Ni nanobelts. It reveals that the real part of the permeability (μ') decreases with increasing frequency in the range of 2–6 GHz and then an abrupt fluctuation from 1 to 1.2 over 6–18 GHz appears. As to the imaginary part of the permeability (μ''), four resonance absorption peaks around 3.8, 5.2, 9.6 and 14.2 GHz are clearly observed, which are denoted as P1, P2, P3, and P4, respectively. Moreover, It is noteworthy that the μ'' rises again with the increasing frequency from 16 to 18 GHz. Therefore, at least one peak may be aroused above 18 GHz. Generally speaking, microwave magnetic loss of magnetic particles originates from hysteresis, domain wall resonance, eddy current effect, natural resonance, and exchange resonance [9]. To our knowledge, the contribution of magnetic hysteresis loss is negligible due to the weak microwave field [5]. Meanwhile, the domain-wall resonance can be excluded in gigahertz range [10]. In this paper, thickness of the nanobelts is thinner than their skin depth. Therefore, the skin effect could also be excluded. Actually, multi-resonance is still a subject of controversy. The most accepted one may be relevant to the present observations of the non-uniform exchange resonance mode [11,12]. In our case, due to the small size effect of the nanobelt and nanocrystalline structure, surface anisotropy and exchange energy would be evidenced [13]. Hence, we assume that the non-uniform magnetic precession still works for our system. As discussed above, the magnetic loss in the Ni nanobelt/paraffin composites should arise from the natural resonance and the exchange resonance, which are discussed later in detail.

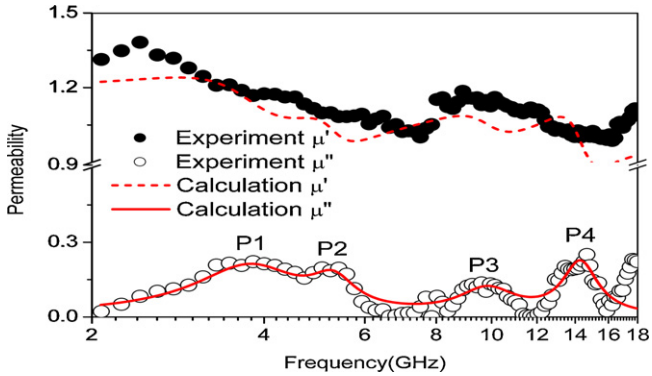

Fig. 2. Experimental and calculated curves of effective permeability of composites consisting of 16.83 vol.% Ni nanobelt.

3.2. Theoretical calculation of the intrinsic permeability for the Ni nanobelts randomly dispersed in paraffin matrix

The LLG equation has been widely used to calculate the dynamic permeability of magnetic materials [14]

$$\frac{d\overline{M}}{dt} = -\gamma(\overline{M} \times \overline{H}) + \frac{\alpha}{M_s}\overline{M} \times \frac{d\overline{M}}{dt}, \quad (1)$$

where $\overline{M}$ represents the magnetization vector; γ is the gyromagnetic factor; α is the damping coefficient; M_s is the saturation magnetization; $\overline{H}$ is the total magnetic field vector.

Exchange coupling effect between neighboring nanograins leads to the parallel arrangement of magnetic moments. Hence, the single domains (nanobelts) are considered in the calculation of the intrinsic permeability. Similar treatment has been demonstrated in Ref. [3]. A simplified diagram in Fig. 3a shows the manners acting between microwave magnetic field (h) and non-geometrical effective in-plane anisotropy field (H_e) in a single Ni nanobelt.The magnetic susceptibility tensor can be expressed as [10]

$$\chi = \begin{pmatrix} \chi_{x'x'} & -i\chi_a & 0 \\ i\chi_a & \chi_{y'y'} & 0 \\ 0 & 0 & 0 \end{pmatrix}, \quad (2)$$

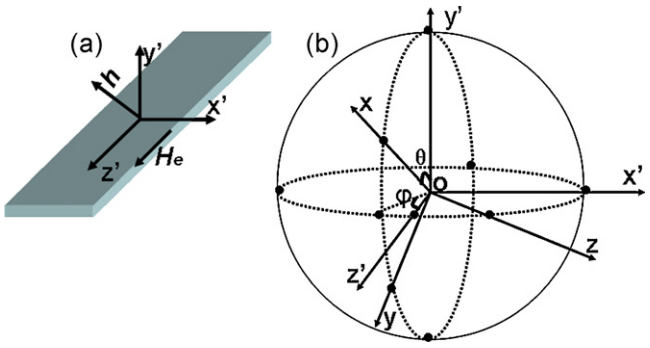

Fig. 3. Coordinate system for microwave propagation in a single Ni nanobelt (a). Two independent Cartesian coordinates: *x*-axis corresponding to the direction of microwave magnetic field; *z*′-axis pointing to the non-geometrical effective in-plane anisotropy field H_e (b).

where

$$\chi_{x'x'} = \frac{\omega_m(\omega_{y'} + i\alpha\omega)}{(\omega_{x'} + i\alpha\omega)(\omega_{y'} + i\alpha\omega) - \omega^2},$$

$$\chi_{y'y'} = \frac{\omega_m(\omega_{x'} + i\alpha\omega)}{(\omega_{x'} + i\alpha\omega)(\omega_{y'} + i\alpha\omega) - \omega^2},$$

$$\chi_a = \frac{-\omega_m\omega}{(\omega_{x'} + i\alpha\omega)\left(\omega_{y'} + i\alpha\omega\right) - \omega^2}.$$

Here, $\omega_{x'} = \gamma H_e + (N_{x'} - N_{z'})\gamma M_s$ and $\omega_{y'} = \gamma H_e + \left(N_{y'} - N_{z'}\right)\gamma M_s$, where $N_{x'}$, $N_{y'}$, $N_{z'}$ are the demagnetizing factors of nanobelt along the x', y', and z' axes, respectively. For a nanobelt with width w, thickness t, the demagnetizing factors can be written as $N_{y'} = 1 - \varepsilon$, $N_{x'} = \varepsilon$, where $\varepsilon = t/w$ [15]. According to the geometrical size of a good number of the practical nanobelts, the average value of ε is estimated to be 0.015.

The intrinsic permeability of the Ni nanobelts randomly dispersed in paraffin matrix can be obtained with the similar approach presented in Ref. [10]. Two independent Cartesian coordinates are given in Fig. 3b. For *o*-*xyz* coordinate system, *x*-axis corresponds to the direction of *h*. In the *o*-*x*′*y*′*z*′ coordinate system, *z*′-axis constantly points to H_e. Accordingly, the microwave magnetization in the *o*-*x*′*y*′*z*′ coordinate system can be written as

$$m_{x'} = x_{x'x'}h_{x'} - i\chi_a h_{y'}, \quad m_{y'} = i\chi_a h_{x'} + \chi_{y'y'}h_{y'}, \quad m_{z'} = 0. \tag{3}$$

In this paper, the direction of H_e keeps stationary, while *h* randomly orients in the space. Based on the randomly generated angles (θ and ϕ) in Fig. 3b, the projections of *h* along the axes of the o-*x*′*y*′*z*′ coordinate system can be expressed as

$$h_{x'} = h\cos(x', x) = -h\sin\theta\sin\varphi, \quad h_{y'} = h\cos(y', x) = h\cos\theta,$$
$$h_{z'} = h\cos(z', x) = h\sin\theta\cos\phi, \tag{4}$$

where (x',x) represents the included angle between x' and x axis and the rest can be deduced by analogy.Combining Fig. 3b with Eqs. (3) and (4), the decompositions of the microwave magnetization to the axes of the *o*-*xyz* coordinate system can be transferred to

$$\begin{aligned}
m_x &= m_{x'}\cos(x', x) + m_{y'}\cos(y', x) = \chi_{x'x'}h\sin^2\theta\sin^2\varphi + \chi_{y'y'}h\cos^2\theta,\\
m_y &= m_{x'}\cos(x', y) + m_{y'}\cos(y', y)\\
&= \chi_{x'x'}h\sin\theta\sin^2\varphi\cos\theta - \chi_{y'y'}h\sin\theta\cos\theta + i\chi_a h\sin\varphi,\\
m_z &= m_{x'}\cos(x', z) + m_{y'}\cos(y', z)\\
&= -\chi_{x'x'}h\sin\theta\sin\varphi\cos\varphi - i\chi_a h\cos\varphi\cos\theta, \text{ where } \cos(x', x)\\
&= -\sin\theta\sin\varphi,\ \cos(y', x) = \cos\theta,\ \cos(x', y)\\
&= -\cos\theta\sin\varphi,\ \cos(y', y) = -\sin\theta,\ \cos(x', z)\\
&= \cos\varphi,\ \cos(y', z) = 0.
\end{aligned} \tag{5}$$

Table 1
Fitted and calculated parameters for permeability dispersion spectra.

Peak	H_e (Oe)	I	a	N	f_c	μ_{kn}	$H_{e(\mathrm{Cal})}$ (Oe)
P1	314.16	0.17	0.14				
P2	635.22	0.06	0.07	0.17	0.34	μ_{11}	944.26
P3	2010.62	0.18	0.12			μ_{12}	1939.19
P4	3279.82	0.33	0.08			μ_{13}	3282.36

With regards to the case of random orientation, the mean values of m_x, m_y, and m_z are given as below

$$\overline{m_x} = \frac{1}{4\pi}\int_0^{\pi}\sin\theta d\theta\int_0^{2\pi}d\phi m_x = \left(\frac{1}{3}\chi_{x'x'} + \frac{1}{3}\chi_{y'y'}\right)h,$$
$$\overline{m_y} = 0,\ \overline{m_z} = 0. \tag{6}$$

Since the measured value is the projection of the permeability along the direction of *h*, the intrinsic permeability is given by

$$\mu_i = 1 + \frac{1}{3}\chi_{x'x'} + \frac{1}{3}\chi_{y'y'}. \tag{7}$$

3.3. Mixing formula of effective permeability

For the composites consisting of Ni nanobelts with arbitrary orientation, the effective permeability is isotropic and given as [16]

$$\mu_{eff} = \mu_m + f\mu_m\frac{\mu_i - \mu_m}{\mu_m + \left(1 - \frac{f}{f_c}\right)N(\mu_i - \mu_m)}, \tag{8}$$

where μ_i and μ_m are the permeability of the inclusion and the matrix, respectively; Here, $\mu_m = 1$ for paraffin; f and f_c are the volume fraction and percolation threshold, respectively; N is the shape factor of inclusions, which is frequently used as a fitting parameter.

4. Results and discussion

Relevant papers have demonstrated that the resonance spectrum could be fitted as a linear superposition of several overlapped resonance curves [9,17–19]. In the present paper, we continue to adapt this approach. The resonance peaks P1–P4 could be separated from each other by fitting the general LLG equation as

$$\mu_i = 1 + \sum_{i=1}^{4} I_i\left[\frac{1}{3}\frac{\omega_m\left(\omega_{y'i} + i\alpha_i\omega\right)}{(\omega_{x'i} + i\alpha_i\omega)\left(\omega_{y'i} + i\alpha_i\omega\right) - \omega^2} + \frac{1}{3}\frac{\omega_m(\omega_{x'i} + i\alpha_i\omega)}{(\omega_{x'i} + i\alpha_i\omega)\left(\omega_{y'i} + i\alpha_i\omega\right) - \omega^2}\right], \tag{9}$$

where I_i is the intensity of the *i*th peak.

The general LLG equation (Eq. (9)) and the modified Maxwell–Garnett mixing rule (Eq. (8)) are used to calculate the intrinsic permeability and the effective permeability, respectively. Firstly, the four resonance peaks in the μ''-*f* curve over 2–16 GHz are fitted. Then the μ'-*f* curve is rebuilt using the obtained fitting parameters, as shown in Fig. 2. All of the fitting parameters are listed in Table 1. As mentioned previously, at least one resonance band above 18 GHz contribute to the μ'-*f* curve. Consequently, the calculated value of μ' is slightly smaller than the experiment result.

Based on the fitting parameters mentioned above, the resonance frequency f_r of the intrinsic permeability for the first peak P1 is 3.65 GHz. To check the mechanism of P1, the Kittel equation [2]

with damping factor α is utilized to calculate the natural resonance frequency as

$$f_r = \frac{\gamma}{2\pi}\left\{\frac{\left[H_e + (N_{x'} - N_{z'})M_s\right]\left[H_e + \left(N_{y'} - N_{z'}\right)M_s\right]}{1+\alpha^2}\right\}^{\frac{1}{2}}. \quad (10)$$

However, H_e is difficult to obtain, since magnetocrystalline anisotropy and magnetic interaction all contribute to the in-plane anisotropy field [17]. Deng et al. suggested using H_c to replace the in-plane anisotropy field [13]. In our case, H_e of the first peak P1 is indeed around H_c. Then the theoretical result of the natural resonance frequency f_r is 3.44 GHz, which matches very well with our calculated result. Therefore, the first peak P1 is mainly attributed to the natural resonance originated from the magnetocrystalline anisotropy, shape anisotropy and magnetic interaction. It is reasonable that the resonance peaks appear in higher frequency range due to the non-uniform exchange resonance modes. According to the exchange resonance mode [11] with the exchange constant $C \approx 1 \times 10^{-7}$ erg/cm, the calculated in-plane anisotropy field $H_{e(cal)}$ accords with the fitting results H_e, when μ_{kn} can be μ_{11}, μ_{12}, and μ_{13} for the resonance peak P2, P3, and P4, respectively, as shown in Table 1. In short, the resonance mechanism originated from the non-uniform magnetic precession theory is generally suitable for our material.

5. Conclusions

In summary, the microwave characterization of Ni nanobelt/paraffin composites is analyzed in the frequency range of 2–18 GHz and four resonance peaks are detected. The combination of the modified LLG equation and Maxwell–Garnett mixing rule is used to predict the effective permeability spectrum of the composites. The computed results indicate that the first band can be ascribed to natural resonance and the following three bands are mainly attributed to the exchange resonance mode. It is believed that the coexistence of natural resonance and exchange resonance is beneficial to enlarge the bandwidth of a microwave absorber.

Acknowledgements

This work was supported by “the Fundamental Research Funds for the Central Universities” and the NSFC (Grant Nos. 61001026 and 51025208).

References

[1] O. Acher, S. Dubourg, Phys. Rev. B 77 (2008) 104440.
[2] C. Kittel, Phys. Rev. 73 (1948) 155–161.
[3] L. Qiao, F.S. Wen, J.Q. Wei, J.B. Wang, F.S. Li, J. Appl. Phys. 103 (2008) 063903.
[4] A.H. Sihvola, Electromagnetic Mixing Formulas and Application, Institution of Electrical Engineers, London, 1999.
[5] L.G. Yan, J.B. Wang, X.H. Han, Y. Ren, Q.F. Liu, F.S. Li, Nanotechnology 21 (2010) 095708.
[6] Z.P. Liu, S. Li, Y. Yang, S. Peng, Z.K. Hu, Y. Qian, Adv. Mater. 22 (2003) 1946–1948.
[7] W.H. Zhong, C.Q. Sun, S. Li, H.L. Bai, E.Y. Jiang, Acta Mater. 53 (2005) 3207–3214.
[8] B. Gao, L. Qiao, J.B. Wang, Q.F. Liu, F.S. Li, J. Feng, D.S. Xue, J. Phys. D: Appl. Phys. 41 (2008) 235005.
[9] J. Ma, J.G. Li, X. Ni, X.D. Zhang, J.J. Huang, Appl. Phys. Lett. 95 (2009) 102505.
[10] S.B. Liao, Ferromagnetic Physics (3), Science, Beijing, 2000.
[11] A. Aharoni, J. Appl. Phys. 69 (1991) 7762–7764.
[12] Ph. Toneguzzo, G. Viau, O. Acher, F. Guillet, E. Bruneton, F.F. Vincent, F. Fievet, J. Mater. Sci. 35 (2000) 3767–3784.
[13] L.J. Deng, P.H. Zhou, J.L. Xie, L. Zhang, J. Appl. Phys. 101 (2007) 103916.
[14] L. Qiao, X.H. Han, B. Gao, J.B. Wang, F.S. Wen, F.S. Li, J. Appl. Phys. 105 (2009) 053911.
[15] J.A. Osborn, Phys. Rev. 67 (1945) 351–357.
[16] K.N. Rozanov, A.V. Osipov, D.A. Petrov, S.N. Starostenko, E.P. Yelsukov, J. Magn. Magn. Mater. 321 (2009) 738–741.
[17] A. Aharoni, Introduction to the Theory of Ferromagnetism, Clarendon, Oxford, 1996.
[18] F. Ma, Y. Qin, Y.Z. Li, Appl. Phys. Lett. 96 (2010) 202507.
[19] F.S. Wen, H.B. Yi, L. Qiao, H. Zheng, D. Zhou, F.S. Li, Appl. Phys. Lett. 92 (2008) 042507.